IEEE Access
Multidisciplinary | Rapid Review | Open Access Journal

Received November 15, 2020, accepted November 24, 2020, date of publication November 30, 2020,
date of current version December 10, 2020.

Digital Object Identifier 10.1109/ACCESS.2020.3041283

Research on the Simplified SVPWM for Three-Phase/Switches Y-Type Two-Level Rectifier

HUI MA[1,2], (Member, IEEE), YUN LU[1], KAITONG ZHENG[1], AND TIANCHUAN XU[1]
[1]College of Electrical Engineering and New Energy, China Three Gorges University, Yichang 443002, China
[2]Chongqing University, Chongqing 404100, China

Corresponding author: Hui Ma (mahuizz119@126.com)

ABSTRACT The three-phase/switch Y-type two-level rectifier is widely used in the unidirectional power-flowing applications such as LED illumination, communication and uninterruptible power supply. This paper presents the working principle of three-phase/switch Y-type two-level rectifier, and proposes two simple and fast modulation techniques (12-sector SVPWM and simplified equivalent SVPWM) based on the virtual vectors. The reference vectors of the 12-sector SVPWM are synthesized by utilizing real basic vectors and virtual vectors linearly combined from these real vectors in a switching period. So the created virtual vectors can reduce the error of reference voltage synthesis, contributing to better input current performance, this paper proposes a simplified 12-sector equivalent SVPWM, and shows the novel three-phase modulation wave expressions and waveforms. The proposed simplified 12-sector equivalent SVPWM does not need the process of sector determination with reducing computational processing time which is attractive for digital implementation. Finally, performance of the proposed modulation methods for a Y-type two-level rectifier using a 5kW prototype is experimentally verified.

INDEX TERMS Carrier modulation, power factor correction circuit, SVPWM, virtual vector.

I. INTRODUCTION

When bidirectional power flux is not necessary, the unidirectional three-phase Y-type two-level rectifier presents some advantages as only using three controllable power transistors which is half of the number of switches in traditional PWM rectifier, no short-circuit phenomenon between bridge arms and smaller processing of energy for the active switches in the application of power unidirectional flow such as LED lighting, communication and uninterruptible power supply. Because of its high sinusoidal current, controllable power factor, effective reduction of switch number and loss, it has promising prospect in the fields of AC/DC electric drive, active power filter, distributed generation, high voltage direct current transmission.

At present, many scholars mainly focus on the control algorithm and pulse width modulation for three-phase/level Vienna-type circuit and multilevel converters. When the DC bus voltage is about twice lower than the rated voltage of the commercial switch, the two-level PFC topology can meet the demand without the need for neutral point potential balance control, which makes the control system simpler. In [6], the discontinuous 2L-SVM strategy of the three-phase three-switch unidirectional rectifier is analyzed and improved on the basis of the discontinuous space vector modulation strategy of the Vienna rectifier. Compared with the continuous 2L-SVM strategy, this strategy reduces the switching loss by 33.33%.

The equivalent relationship between carrier-based pulse width modulation and SVPWM provides a platform not only to transform from one to another, but also to develop lots of PWM modulators. The unified theoretical analysis and verification between SVPWM and SPWM were carried out, and the equivalent space vector modulation can be easily got by injecting zero sequence component or common mode injection. Numerous researchers have verified that the equivalent SVPWM can optimize the control effect for converters. Reference [7] proposed a generated decomposi-tion method to obtain the accurate injected zero component, and this theoretical derivation can be extended to acquire the accurate zero component expression for the Y-type two-level rectifier. In [8], a new carrier-based pulse width modulation strategy was proposed to achieve the nearest three-vector SVPWM strategy, which reduced the switching loss and the

The associate editor coordinating the review of this manuscript and approving it for publication was Xiaojun Bi.

low frequency voltage oscillation of the neutral point. Additionally, the synchronized SVPWM is designed for three-level converters, which achieves this function in the following way that the switching sequences and two reference vector distribution modes are designed at each segmentation independently, and this synchronized SVPWM can improve the output waveforms while reducing the device switching frequency. The above references discussed the equivalent relationship between SVPWM and SPWM for three-level voltage source rectifier (VSR) and VIENNA-type rectifier, and the equivalence between SVPWM and SPWM is realized by the well-known third harmonic injection principle. However, the operation mode of Y-type two-level rectifier is different from the traditional PWM converter, so the PWM converter's zero sequence component cannot be directly applied to Y-type two-level rectifier. According to the combination states of the three active switches, two novel pulse width space-vector modulations are designed for Y-type two-level rectifier.

In order to acquire the simplified SVPWM for the unidirectional Y-type two-level PFC. Firstly, the working principle of Y-type PFC and the design process of virtual vectors are deduced in detail, then a 12-sector SVPWM is proposed to simplify process of sector division using virtual vectors. Compared with the traditional 6-sector SVPWM, the novel 12-sector SVPWM will increase the number of switching operations when it is used to synthesize the target reference vector, but it can effectively reduce the error between the target synthesized voltage and the reference voltage, so it can reduce the input current ripple. Second, in order to overcome the more controller resource occupied by sector judgment and basic vector acting time calculation in the 12-sector SVPWM, based on the equivalent relationship between SVPWM and SPWM, the simplified 12-sector SVPWM is proposed by using the three-phase duty cycle functions, and this paper gives the detailed derivation process, the expressions of the equivalent 12-sector SVPWM in table form and the simulation waveforms. Finally, performance of the proposed two 12-sector SVPWM strategies for the unidirectional three-phase Y-type two-level rectifier, based on the simulation studies and experiments in the 5kW prototype, are demonstrated the validity and effectiveness of the theoretical analysis by the simulation and experimental results.

II. WORKING PRINCIPLE OF Y-TYPE TWO-LEVEL PFC

Three-phase Y-type PFC circuit is shown in Fig. 1. $u_a u_b u_c$ are three-phase input voltages, $i_a i_b i_c$ are three phase input currents, $i_p i_n$ are positive and negative dc-bus current. $L_a L_b L_c$ are three-phase filter inductors with a value of L, $R_a R_b R_c$ are the equivalent resistance of the circuit, R_L is the output load. $S_a S_b S_c$ is the switch function of three-phase PFC circuit. A bidirectional switch and two fast recovery diodes form a phase bridge arm, in which the bidirectional switch consists of a MOSFET with four diodes as shown in the right of Fig. 1. The three-switch two-level PFC based on MOSFET is a voltage driven circuit, whose output voltage at both ends of the main control power device is determined by input current direction and the on/off state of active switches.

The Y-type two-level PFC is a power unidirectional flow circuit. According to the input-current direction, the operation mode of any phase bidirectional switch is analyzed, its current path is shown in Fig. 2. During the positive half cycle of the input current, when the switch is on, the current flows through D_{k1} and D_{k4}, while when the switch is off, the current only flows through D_{k1}, that is means this circuit has no short-circuit phenomenon between two bridge arms, and the negative half cycle current path is symmetrical with the above path. The switch of each bridge arm has two states: on and off, and there are 8 combinations of three-bridge arms. According to the direction of the voltage and current, seven basic vectors of the circuit are obtained as shown in Table 1, and "−" in Table 1 indicates any current direction.

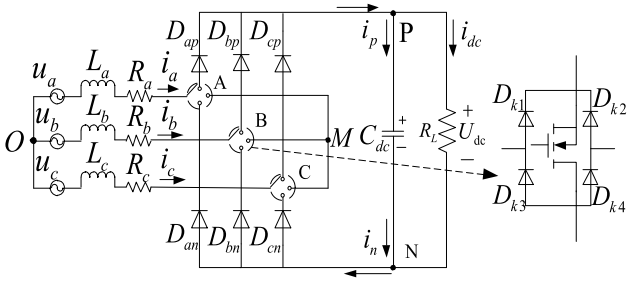

FIGURE 1. Topology of three-phase three-switch two-level PFC.

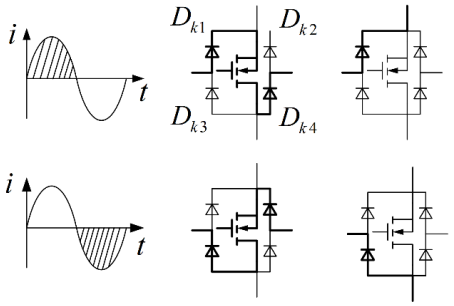

FIGURE 2. The current working path of the bidirectional switch

TABLE 1. The Seven Basic Vectors.

Current direction			Switch connection point			Basic vector
i_a	i_b	i_c	A	B	C	
-	-	-	M	M	M	$\vec{V}_0$ (000)
>0	<0	<0	P	N	N	$\vec{V}_1$ (100)
>0	>0	<0	P	P	N	$\vec{V}_2$ (110)
<0	>0	<0	N	P	N	$\vec{V}_3$ (010)
<0	>0	>0	N	P	P	$\vec{V}_4$ (011)
<0	<0	>0	N	N	P	$\vec{V}_5$ (001)
>0	<0	>0	P	N	P	$\vec{V}_6$ (101)

Each leg of the Y-type PFC has three common connection points M, P and N, as shown in Fig. 1. In order to effectively analyze the working state of the circuit, the switch function is

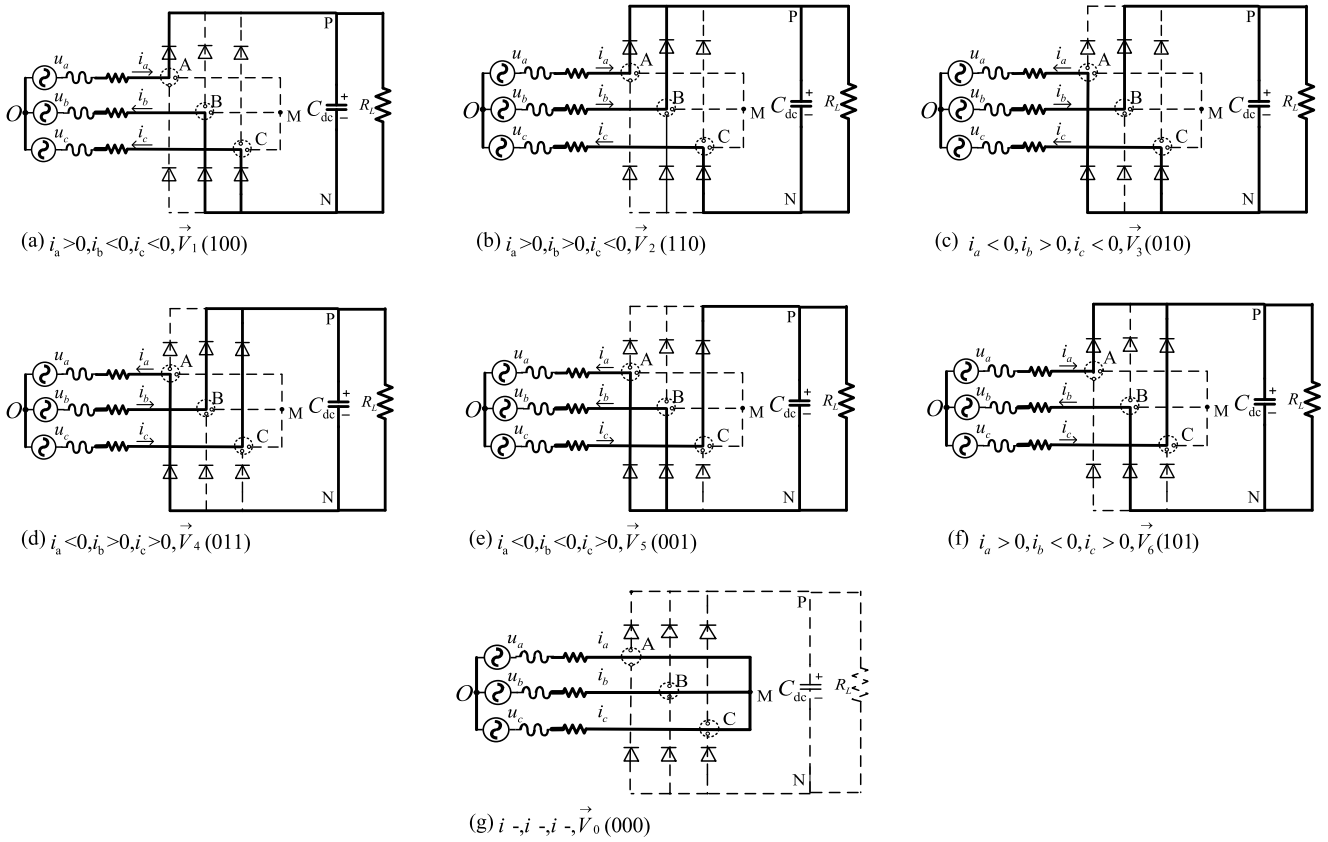

FIGURE 3. The seven basic vectors of the Y-typed PFC.

defined as follows: when the point of each phase arm (A, B, C) is connected with P, the switching function is defined as 1. When it is connected with N and M, the switching function is defined as 0.

Seven topological stages may be performed from basic operation mode as shown in Table 1, among them, the basic vector (000) is a redundant vector, which is only used to adjust the action time of different basic vectors, its mode is not limited by the current direction, and it only has one working condition connected with M. For the seven basic vector modes, the working states of the circuit are shown in Fig.3 and they are shown as follows:

(a) State 1 [Refer to Fig. 3(a)]: S_a is turned on, and the other two switches are turned off. The active current path of this mode is shown in Fig. 3(a). During this state, $U_{AB} = +U_{dc}$, $U_{BC} = 0$, $U_{CA} = -U_{dc}$, and phase A current decreases, phase B current increases when the line voltage U_{AB} is greater than 0.

(b) State 2 [Refer to Fig.3(b)]: S_c is turned on, and the other two switches are turned off. The active current path of this mode is shown in Fig. 3(b). During this state,$U_{AB} = 0$, $U_{BC} = +U_{dc}$, $U_{CA} = -U_{dc}$, phase A and phase B currents increase, and $i_a+i_b+i_c = 0$, thus, phase C current decreases.

(c) State 3 [Refer to Fig. 3(c)]: S_b is turned on, and the other two switches are turned off. The active current path of this mode is shown in Fig. 3(c). During this state, $U_{AB} = -U_{dc}$, $U_{BC} = +U_{dc}$, $U_{CA} = 0$, and phase B current decreases, phase C current increases when the line voltage U_{CA} is greater than 0. Capacitor C_{dc} is in a state of charge.

(d) State 4 [Refer to Fig. 3(d)]: S_a is turned on, and the other two switches are turned off. The active current path of this mode is shown in Fig. 3(d). During this state, $U_{AB} = -U_{dc}$, $U_{BC} = 0$, $U_{CA} = +U_{dc}$, phase B and phase C currents decreases, and $i_a + i_b + i_c = 0$, thus, phase A current increases.

(e) State 5 [Refer to Fig. 3(e)]: S_c is turned on, and the other two switches are turned off. The active current path of this mode is shown in Fig. 3(e). During this state, $U_{AB} = 0$, $U_{BC} = -U_{dc}$, $U_{CA} = +U_{dc}$, and phase C current decreases, phase A current increases when the line voltage U_{AB} is greater than 0. Capacitor C_{dc} is in a state of charge.

(f) State 6 [Refer to Fig. 3(f)]: S_b is turned on, and the other two switches are turned off. The active current path of this mode is shown in Fig. 3(f). During this state, $U_{AB} = +U_{dc}$, $U_{BC} = -U_{dc}$, $U_{CA} = 0$, phase A and phase C currents decreases, and $i_a+i_b+i_c = 0$, thus, phase B current increases.

(g) State 7 [Refer to Fig. 3(g)]: This state works in redundant vector mode. Zero output in this state, $U_{AB} = U_{BC} = U_{CA} = 0$.

III. 12-SECTOR SVPWM BASED ON VIRTUAL VECTOR

A. PRINCIPLE ANALYSIS OF 12-SECTOR SVPWM

It is needed to consider the direction of current with the realization of effective basic vector in unidirectional power-flow circuit, that is, the power switch works in the same direction of voltage and current, so the SVPWM sector division of three-phase PFC based on unidirectional power flow is different from the traditional PWM rectifier.

The voltage vectors, voltage states and sector division are shown in Fig. 4 and Fig. 5. For SVPWM based on 12-sector, there are 12 voltage vectors, consist of six basic real vectors $\vec{V}_1\vec{V}_2\vec{V}_3\vec{V}_4\vec{V}_5\vec{V}_6$, six virtual vectors $\vec{V}_{1,2}\vec{V}_{2,3}\vec{V}_{3,4}\vec{V}_{4,5}\vec{V}_{5,6}\vec{V}_{1,6}$ which be generated with the linear combination of real voltage vectors. These virtual vectors can greatly increase the number of voltage vectors on the AC side, effectively reduce the error between the reference voltage vector and the synthesis target voltage vector, and improve the input current performance. The sector division based on 12-sector SVPWM is different from the traditional 6-sector division in that the real vectors and virtual vectors divide the operational sectors every 30°, so that the voltage vector space is divided into 12 sectors[18].

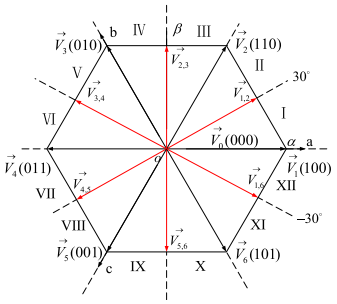

FIGURE 4. Space vector distribution of the Y-type PFC.

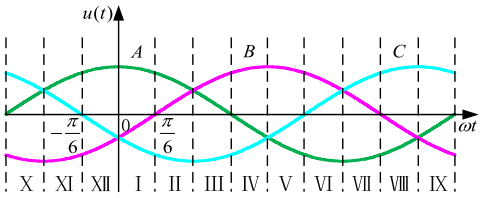

FIGURE 5. The 12-Sector Division.

The three-phase input voltage is divided into 12 cycles in one power frequency cycle based on the zero-crossing point and the intersection of three-phase input voltage as shown in Fig. 5. Based on the tangent value of $\alpha\beta$ coordinate, the sector judgment can be carried out, it can be named as:

$$\tan\alpha = u_\beta / u_\alpha \tag{1}$$

where u_α and u_β are the reference input voltage of the rectifier in $\alpha\beta$ coordinate. The specific conditions of sector judgment are shown in Table 2.

TABLE 2. Sector Conditions of 12-Sector Svpwm.

Sector	Judgment conditions
I	$\sqrt{3}u_\beta - u_\alpha < 0 \,\&\, u_\alpha > 0, u_\beta > 0$
II	$\sqrt{3}u_\beta - u_\alpha > 0 \,\&\, \sqrt{3}u_\alpha - u_\beta > 0$
III	$\sqrt{3}u_\alpha - u_\beta < 0 \,\&\, u_\alpha > 0$
IV	$\sqrt{3}u_\alpha + u_\beta > 0 \,\&\, u_\alpha < 0$
V	$\sqrt{3}u_\alpha + u_\beta < 0 \,\&\, \sqrt{3}u_\beta + u_\alpha < 0$
VI	$\sqrt{3}u_\beta + u_\alpha > 0 \,\&\, u_\beta > 0$
VII	$\sqrt{3}u_\beta - u_\alpha > 0 \,\&\, u_\beta < 0$
VIII	$\sqrt{3}u_\beta - u_\alpha < 0 \,\&\, u_\beta - \sqrt{3}u_\alpha > 0$
IX	$u_\beta - \sqrt{3}u_\alpha < 0 \,\&\, u_\alpha < 0$
X	$\sqrt{3}u_\alpha + u_\beta < 0 \,\&\, u_\alpha > 0$
XI	$\sqrt{3}u_\alpha + u_\beta > 0 \,\&\, \sqrt{3}u_\beta + u_\alpha < 0$
XII	$\sqrt{3}u_\beta + u_\alpha > 0 \,\&\, u_\alpha > 0, u_\beta < 0$

The virtual vector is linearly combined by two real vectors in one switching cycle, which can be realized by comparing the three-phase duty cycle with the triangular carrier. The specific synthesis method is shown in Table 3.

TABLE 3. Virtual Vector Synthesis.

Virtual vectors	Synthesised style	Three phase duty cycle
$\vec{V}_{1,2}$	$0.5\vec{V}_1 + 0.5\vec{V}_2$	1,0.5,0
$\vec{V}_{2,3}$	$0.5\vec{V}_2 + 0.5\vec{V}_3$	0.5,1,0
$\vec{V}_{3,4}$	$0.5\vec{V}_3 + 0.5\vec{V}_4$	0,1,0.5
$\vec{V}_{4,5}$	$0.5\vec{V}_4 + 0.5\vec{V}_5$	0,0.5,1
$\vec{V}_{5,6}$	$0.5\vec{V}_5 + 0.5\vec{V}_6$	0.5,0,1
$\vec{V}_{1,6}$	$0.5\vec{V}_1 + 0.5\vec{V}_6$	1,0,0.5

Take the virtual vectors $\vec{V}_{1,2}\vec{V}_{2,3}$ for example, the synthesis principle is shown in Fig. 6. In the Fig. 6, the amplitude of triangular carrier is 1, and the switching frequency is T_s . So it can be seen from the Fig. 6, the vector sequences output by the virtual vectors $\vec{V}_{1,2}$ and $\vec{V}_{2,3}$ in one switching cycle are $\vec{V}_1 - \vec{V}_2 - \vec{V}_1$, $\vec{V}_3 - \vec{V}_2 - \vec{V}_3$, respectively. Based on the above synthesis principle, more virtual vectors can be obtained by the real vectors in the vector space.

It can be seen from Fig. 7(b) and Table 3 that the output information of PLL can be unified with the sector division, and the judgment conditions are clear and easy to understand. Based on the unidirectional power flow and two-level characteristics of the Y-type PFC circuit, a five-segment symmetrical SVPWM modulation mode is adopted in order to make the control signal be the same at the beginning and end of the switching cycle, lessen the switching action times and

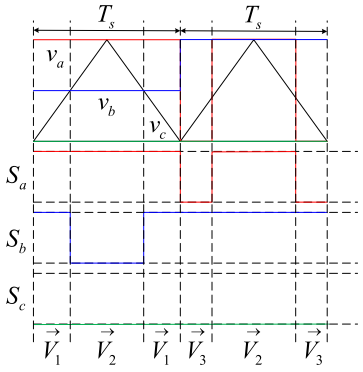

FIGURE 6. The synthetized principle of virtual vectors $\vec{V}_{1,2}\vec{V}_{2,3}$.

reduce the harmonic content. In each sector, the zero vector $\vec{V}_0$ first acts on the synthesis target vector, through the orderly combination of the switch sequence of the adjacent sector, only one switch is turned on at each time, according to which the switch sequence in each sector can be designed. Taking the first sector as an example, when the voltage reference vector locates in the first sector, the schematic diagram of synthesizing $\vec{V}_{ref}$ with the virtual voltage vector is shown as Fig. 8.

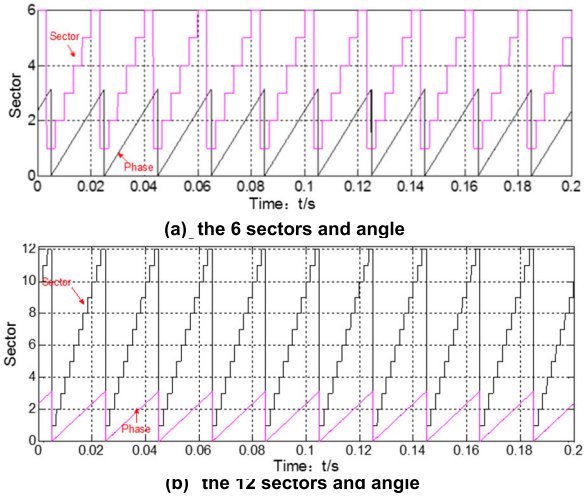

FIGURE 7. The simulation diagrams of 6-sector and 12-sector.

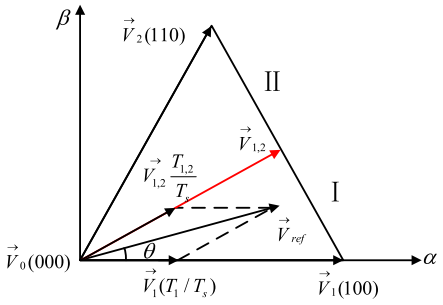

FIGURE 8. Schematic diagram of voltage vector synthesis.

According to the nearest vector synthesis principle, three basic vectors $\vec{V}_0\vec{V}_1\vec{V}_{1,2}$ are closest to the reference vector who are selected to synthesize the $\vec{V}_{ref}$, the acting time of these basic vector is $T_0T_1T_{1,2}$ respectively. According to the volt-second principle, the effective basic vector action time equation can be obtained as follows:

$$\begin{cases} T_1V_1 + T_{1,2}V_{1,2} = T_sV_{ref} \\ T_1 + T_{1,2} + T_0 = T_s \end{cases} \tag{2}$$

By projecting virtual vector into two adjacent vectors, we can get:

$$\begin{cases} |V_\alpha|\,T_s = |V_1|\,T_1 + (\sqrt{3}/2)\,|V_{1,2}|\,T_{1,2} \\ |V_\beta|\,T_s = (|V_{1,2}|\,T_{1,2})/2 \\ T_s = T_1 + T_{1,2} + T_0 \end{cases} \tag{3}$$

According to the $|V_{dc}|$, the amplitude of vectors $\vec{V}_1$ and $\vec{V}_{1,2}$ are standardized in $\alpha\beta$ coordinate system, and their length are $2V_{dc}/3$, $\sqrt{3}\,V_{dc}/3$,respectively. Finally, in sector I, the acting time of each vector can be obtained as:

$$\begin{cases} T_{1,2} = \left(2\sqrt{3}\,V_\beta T_S\right)/V_{dc} \\ T_1 = 3(V_\alpha T_s - \sqrt{3}\,V_\beta T_s)/2V_{dc} \\ T_0 = T_s - T_{1,2} - T_1 \end{cases} \tag{4}$$

Table 3 is used to calculate and allocate the action time of each vector state, and the following equation is obtained:

$$\begin{cases} T_{(100)} = T_1 \\ T_{(110)} = 2T_{1,2} - T_1 \end{cases} \tag{5}$$

Fig. 9 shows the sequence diagram of the switch drive signal for one switch cycle in the first sector.

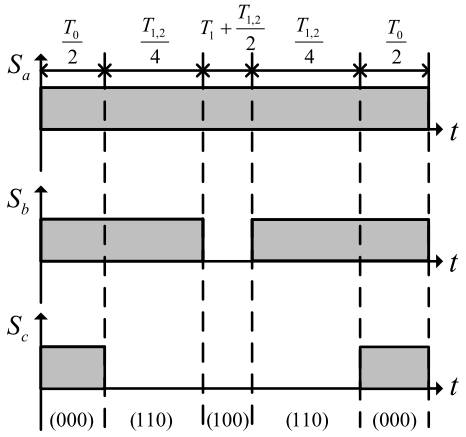

FIGURE 9. Sector I switch driving signal sequence diagram.

B. ANALYSIS OF VOLTAGE AND CURRENT CHARACTERISTICS

The six virtual vectors proposed in this paper can be generated with the linear combination of real voltage vectors, which can increase the number of finite control sets ($V_{ref\alpha}$ and $V_{ref\beta}$) in the reference voltage synthesis and improve the control

domain and utilization ratio of vector space, thus the error in reference vector synthesis is reduced effectively and the control accuracy is improved. In this paper, the modulation strategy is analyzed in two aspects: voltage error and harmonic current [19]. The total voltage error of the 6-vector modulation and 12-vector modulation strategies are analyzed. The total voltage-vector error is defined as:

$$g_{ve} = \sqrt{(V_{ref\alpha} - V_{v\alpha})^2 + (V_{ref\beta} - V_{v\beta})^2} \tag{6}$$

In the (6), $V_{ref\alpha}$ and $V_{ref\beta}$ are the components of reference voltage vector $\vec{V}_{ref}$ in $\alpha\beta$ coordinate system, respectively. $V_{v\alpha}$ and $V_{v\beta}$ are the components of the three-phase PFC synthetic target vector in the $\alpha\beta$ coordinate system. In each sampling period, the reference vector points in a sector are sampled, and the voltage error is calculated by the (6). Taking the total voltage error of sector I in time $\pi/4$ as an example, the total voltage error under different sector division methods is shown in Fig. 10. It can be seen from the Fig. 10 that the total voltage error of 12-sector SVPWM is less than that of 6-sector SVPWM with different modulation ratios, which indicates that the virtual vector can reduce the error of synthesizing target vector.

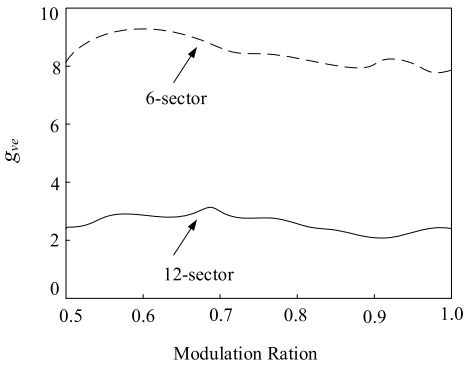

FIGURE 10. Total voltage error of 6-sector and 12-sector.

Fig. 11 shows the simulation diagram of $V_{ref\alpha}$ and $V_{ref\beta}$ trace under the 6-sector division mode and 12-sector division mode. In order to compare the influence of different sector division modes on the switching voltage trajectory more clearly, and the sampling frequency of the switching frequency is 12kHz, and the total simulation time is 0.08s. Compare and analyze the Fig. 11 (a) and Fig. 11 (b), it can be seen that the switching voltage track distortion of the three-phase PFC based on the division of 6-sector is more serious, and the amplitude fluctuation of the switching voltage is larger, while the circuit shows better performance in the division mode of 12-sector, its switching voltage track is closer to the circle, and the track distortion is significantly reduced.

In this paper, the RMS value of current ripple is selected as the performance index, and the calculation method of harmonic current based on fourier transform is adopted, which ignores the related loss in the circuit to simplify the calculation process. Taking the calculation of A-phase harmonic current as an example, the current ripple expression in the time period T_1 is as follows:

$$\Delta i_a(t) = \frac{V_{dc} - u_a}{L_a} t = \frac{V_{dc}}{L_a}(1 - m)t \tag{7}$$

In the (7), $m = u_a/V_{dc}$, the expression of ripple current in time period T_2 is given as:

$$\begin{aligned}\Delta i_a(t) &= \frac{(V_{dc} - u_a)}{L_a} T_1 - \frac{(V_{dc} + u_a)}{L_a}(t - T_1) \\ &= \frac{V_{dc}}{L_a}\left[(1 - m)T_1 - (1 + m)(t - T_1)\right] \\ &\quad (T_1 < t < T_1 + T_2)\end{aligned} \tag{8}$$

Fig. 12 shows the switch pulse and ripple current of the A-phase bridge arm. In Fig. 11, if the integral variable is set as $x = t - T_1$ in half a switching period, the RMS value of harmonic current is as follows[20]:

$$\begin{aligned}\Delta i_a^2 = \left(\frac{V_{dc}}{La}\right)^2 \frac{T_S}{2} \Bigg(&\int_0^{T_1} (1 - m)^2 t^2 dt \,) \\ &+ (\int_0^{T_2} [(1 - m)T_1 - (1 + m)x]^2 dx \Bigg)\end{aligned} \tag{9}$$

Equation (9) can be further simplified as:

$$\Delta i_a^2 = (\frac{V_{dc}}{L_a})^2 (1 - m^2)^2 \frac{T_S^2}{48} \tag{10}$$

Then the effective value of harmonic current in one switching period is:

$$I_{hc} = \sqrt{\Delta i_a^2} = \frac{V_{dc}}{L_a}(1 - m^2)\frac{T_S}{4\sqrt{3}} \tag{11}$$

IV. NEW EQUIVALENT SVPWM BASED ON Y-TYPE PFC CIRCUIT

In order to improve the voltage utilization and simplify the complex calculation process of traditional SVPWM, the third harmonic component is injected into the sinusoidal modulation wave to form the saddle wave, which is equivalent to the space-vector pulse width modulation. In addition, since the working mode of this PFC circuit is different from the traditional two-level rectifier, it can be seen from the the previous analysis of its working principle that the circuit working mode is more flexible, that is, in the outputting the same basic vector, it has a variety of switching combinations. When the new modulation waves synthesized, it is necessary to comprehensively consider the direction of current, and the principle of the less-switching times.

In [4], the essential relationship between SVPWM and SPWM is studied in detail, and the zero sequence component of three-phase converter is theoretically derived and simulated, which can provide a theoretical basis of the realization of equivalent SVPWM for Y-type two-level PFC. The space-vector coordinate values in two-phase static coordinate system are shown in Fig. 13, which can be obtained from

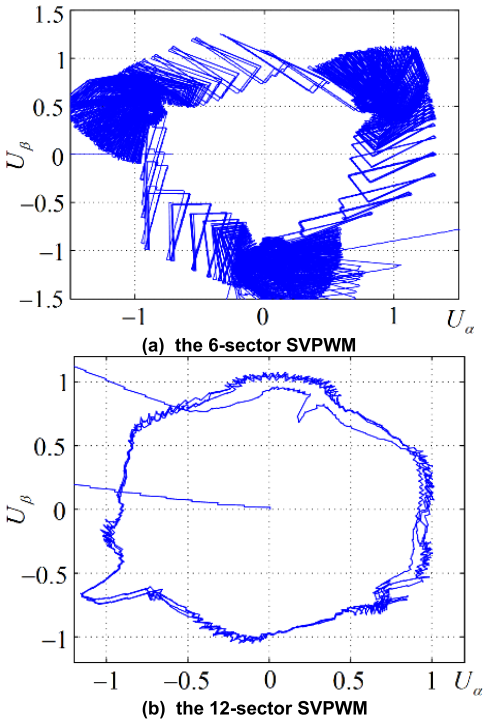

FIGURE 11. $V_{ref\alpha}$, $V_{ref\beta}$ traces in $\alpha\beta$ coordinate system.

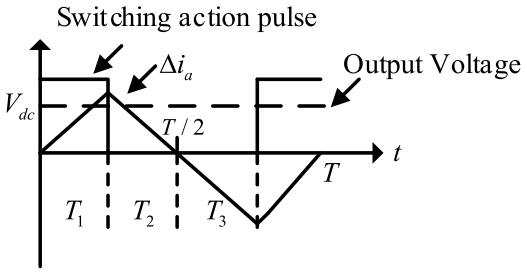

FIGURE 12. Switching action pulse and ripple current in one period.

three-phase coordinate system by using Clark transformation matrix. Taking sector I as an example, the (2) can be rewritten by using virtual vectors and real vectors in the Table 3 as shown:

$$\begin{aligned} T_s\vec{V}_{ref} &= T_1'\vec{V}_1 + T_2'\vec{V}_2 \\ &= (T_1 + \frac{T_{1,2}}{2})V_1 + \frac{T_{1,2}}{2}\vec{V}_2 \end{aligned} \tag{12}$$

By substituting the vector coordinates in $\alpha\beta$ coordinate system into (12), it can be obtained:

$$\begin{aligned} T_s\vec{V_{ref}} &= \sqrt{2/3}\vec{V}_\alpha \cdot T_1' + (1/\sqrt{6}\vec{V}_\alpha \\ &+\sqrt{2}/2\vec{V}_\beta) \cdot T_2' = T_\alpha \cdot \vec{V}_\alpha + T_\beta \cdot \vec{V}_\beta \end{aligned} \tag{13}$$

The coordinate components on both sides of the (13) are equal, and the action time of basic vectors $\vec{V}_1$, $\vec{V}_2$ can be determined when the reference vector $V_{ref\alpha}$ in $\alpha\beta$ coordinate

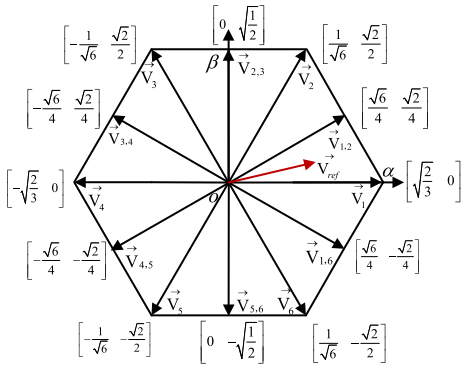

FIGURE 13. Space vector in $\alpha\beta$ coordinate system.

system is located in sector I:

$$\begin{cases} T_1' = \sqrt{3/2}T_\alpha - \sqrt{2}/2T_\beta \\ T_2' = \sqrt{2}T_\beta \end{cases} \tag{14}$$

In sector I, the proposed vector sequence is $\vec{V}_0\vec{V}_2\vec{V}_1\vec{V}_2\vec{V}_0$, resulting in the drive signals in Fig. 9. Therefore, the intervals for the commands of switches are:

$$T_a = T_s, T_b = T_0 + T_2', T_c = T_0 \tag{15}$$

Using the duty cycle in the $\alpha\beta$ coordinate system, the new modulated wave in the three-phase coordinate system can be described as follows:

$$\begin{cases} v_a^* = 1 \\ v_b^* = 1 - \sqrt{3/2}D_\alpha + D_\beta \\ v_c^* = 1 - \sqrt{3/2}D_\alpha + 1/\sqrt{2}D_\beta \end{cases} \tag{16}$$

In the (16), $D_\alpha = T_\alpha/T_s, D_\beta = T_\beta/T_s$. Using the above methodology for all sectors, it can be deduced that the duty cycle expressions of all sectors. Sector I and XII, II and III, IV and V, VI and VII, VIII and IX, X and XI are the same, as shown in Table 4.

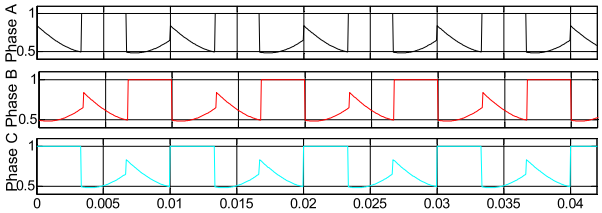

FIGURE 14. The three-phase modulation waves.

Fig. 14 shows the newly synthesized three-phase modulation waves, which are compared with the triangular carrier to output the switching logic signal directly. The equivalent SVPWM based on the new three-phase modulation wave is simple, and no sector judgment and vector action time calculation are needed, which can reduce greatly computational processing time which is its simplicity for digital implementation. Comparing between the two-level SPWM

TABLE 4. The New Modulation Wave of Each Sector.

SECTORS	THREE-PHASE MODULATED WAVE
I & XII	$v_a^* = 1$ $v_b^* = 1 - \sqrt{3/2}D_\alpha + 1/\sqrt{2}\,D_\beta$ $v_c^* = 1 - \sqrt{3/2}D_\alpha - 1/\sqrt{2}\,D_\beta$
II & III	$v_a^* = 1 - \sqrt{3/2}D_\alpha + 1/\sqrt{2}\,D_\beta$ $v_b^* = 1$ $v_c^* = 1 + \sqrt{2}D_\beta$
IV & V	$v_a^* = 1 + \sqrt{3/2}D_\alpha + 1/\sqrt{2}\,D_\beta$ $v_b^* = 1 + \sqrt{2}D_\beta$ $v_c^* = 1$
VI & VII	$v_a^* = 1$ $v_b^* = 1 + \sqrt{3/2}D_\alpha - 1/\sqrt{2}\,D_\beta$ $v_c^* = 1 + \sqrt{3/2}D_\alpha + 1/\sqrt{2}\,D_\beta$
VIII & IX	$v_a^* = 1 + \sqrt{3/2}D_\alpha - 1/\sqrt{2}\,D_\beta$ $v_b^* = 1$ $v_c^* = 1 - \sqrt{2}D_\beta$
X & XI	$v_a^* = 1 - \sqrt{3/2}D_\alpha - 1/\sqrt{2}\,D_\beta$ $v_b^* = 1 - \sqrt{2}D_\beta$ $v_c^* = 1$

and the space-vector modulation in sector I and III, and it is illustrated in Fig. 15, the $v_a^* v_b^* v_c^*$ are three-phase equivalent modulation waves injected with zero-sequence component, $T_a T_b T_c$ are the time when the modulation amplitude is larger than the carrier amplitude, that is, the time when the three-phase of A, B and C output high potential in one modulation period, and $t_0 t_1 t_2$ are the action time of the vectors $\vec{V}_0 \vec{V}_1 \vec{V}_2$ in the space vector modulation, respectively. The upper part of Fig. 15 is the switch timing sequence of SVPWM, and the lower part of Fig. 15 is about the comparison between the new modulation wave and the carrier wave. It can be concluded that SVPWM is equivalent to SPWM based on the new modulation wave.

V. EXPERIMENTAL RESULTS

The performance of the proposed 12-sector SVPWM and the new modulation technology based on equivalent SVPWM were verified using a 5-kW three-phase two-level PFC experimental platform, and the experimental circuit is shown as the Fig. 16. The specific parameters of the circuit are shown in Table V. DSP-TMS320F28335 is used as the experimental controller, the bidirectional switch is SKM60GM123 and the fast recovery diode is DSEI2 101-12A. The three-phase power input is provided by the three-phase voltage regulator TSGC2-9, and the relevant measuring equipment is as follows: the oscilloscope is DS1104, the high-voltage probe is GENTEK-G3100.

Fig. 17 shows the sector, phase angle and the A-phase voltage and current waveforms of 12-sector modulation

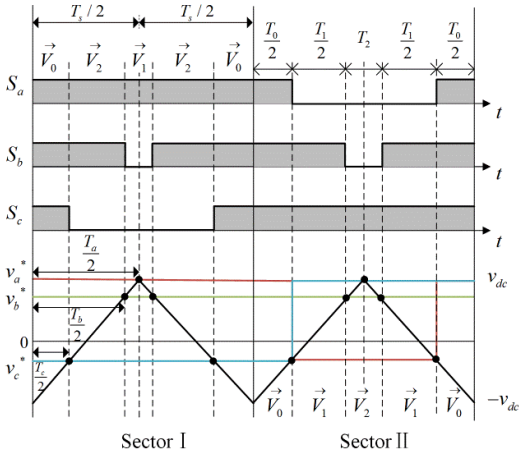

FIGURE 15. The novel SVPWM in sector I and I.

TABLE 5. Main Parameters of the Circuit.

Description	Value
RMS input voltage	220V
Output voltage	650V
Input inductor	2.4mH
Switching frequency	12kHz
Output capacitor	3300μF
Output power	5kW

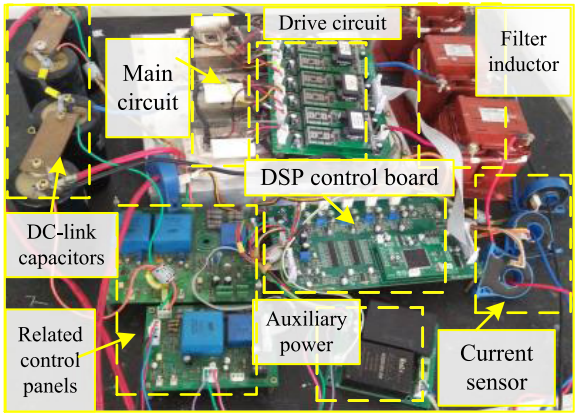

FIGURE 16. The experimental circuit.

and 6-sector modulation, respectively. When measuring the experimental voltage and current waveforms of A phase, the oscilloscope probe is set to twice the coefficient. Fig. 17(a) shows the relationship between the six sectors and the Phase angle of the 6-sector modulation. Due to the influence of the parasitic parameters in the actual circuit and the accuracy of the sampling circuit of the controller, the experimental waveform has an acceptable small error, which is consistent with the simulation results of the Fig. 7(a). Fig. 17(b) shows the experimental voltage and current waveforms of A-phase, the Y-type rectifier operates with

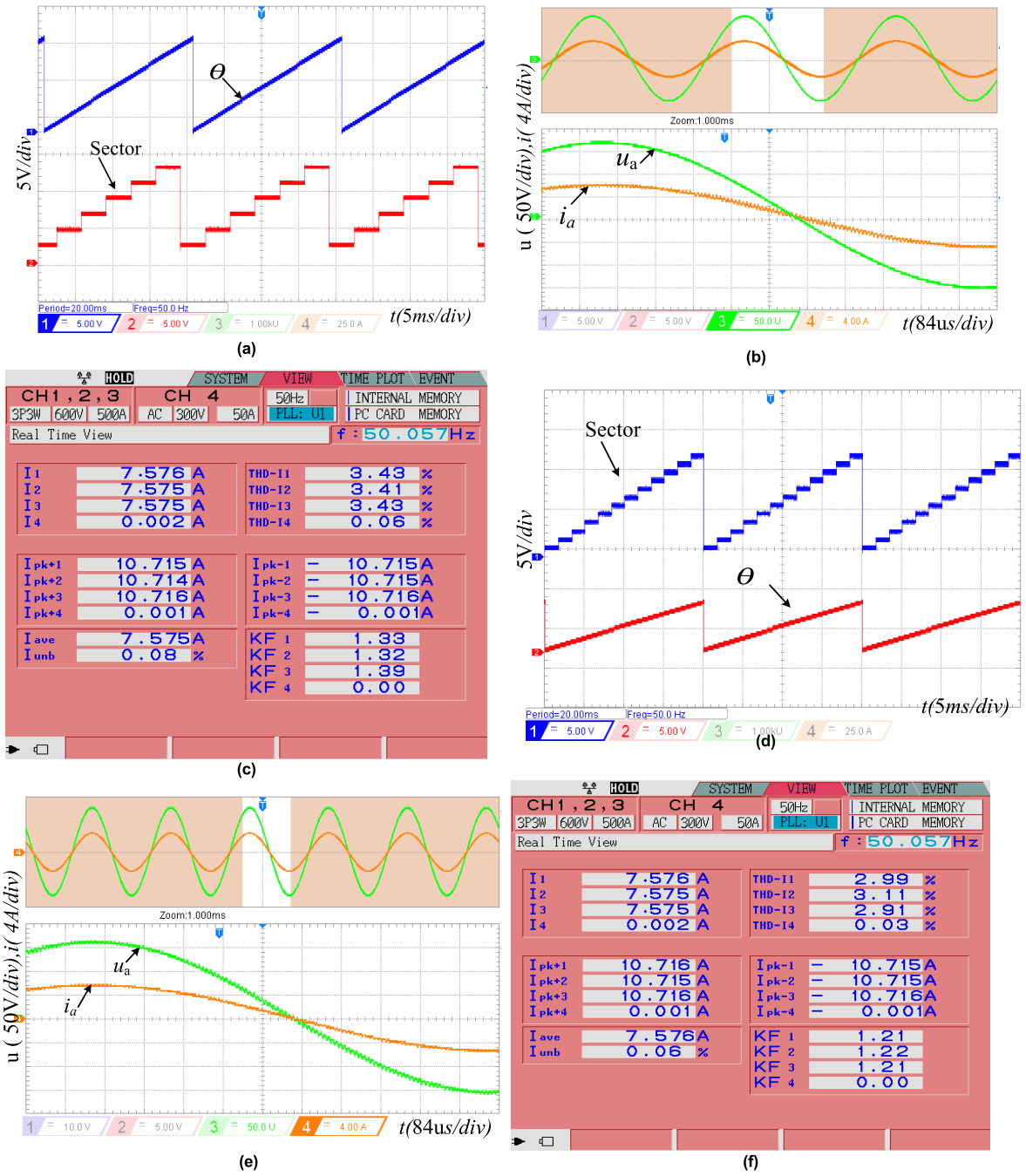

FIGURE 17. The sector and phase angle,the A-phase voltage and current waveforms and the three-phase current THD. The 6-sector modulation: (a) the sector and phase angle, (b) A-phase voltage and current waveforms, (c) the three-phase current THD; The 12-sector modulation: (d) the sector and phase angle, (e) A-phase voltage and current waveforms, (f) the three-phase current THD.

sinusoidal current waveform and unit power factor. Fig. 17(c) shows the harmonic analysis of three-phase current, and the average total harmonic distortion (THD) of three-phase current is about 3.3%. The current harmonic contents of the 6-sector modulation technology meets the related requirements. Fig. 17(d), Fig. 17(e) and Fig. 17(f) show the sector, phase information and the A-phase voltage and current waveforms of 12-sector modulation. The relationship between the sectors and the Phase angle of the 12-sector modulation is consistent with the simulation results of the Fig. 7(b). Compare and analyze Fig. 17(b) and Fig. 17(e), It can be concluded that the current waveform of 12-sector modulation has high smoothness and small ripple. Fig. 17(f) shows the harmonic analysis of three-phase current based on the 12-sector modulation, and the average THD of three-phase current is about 3%.

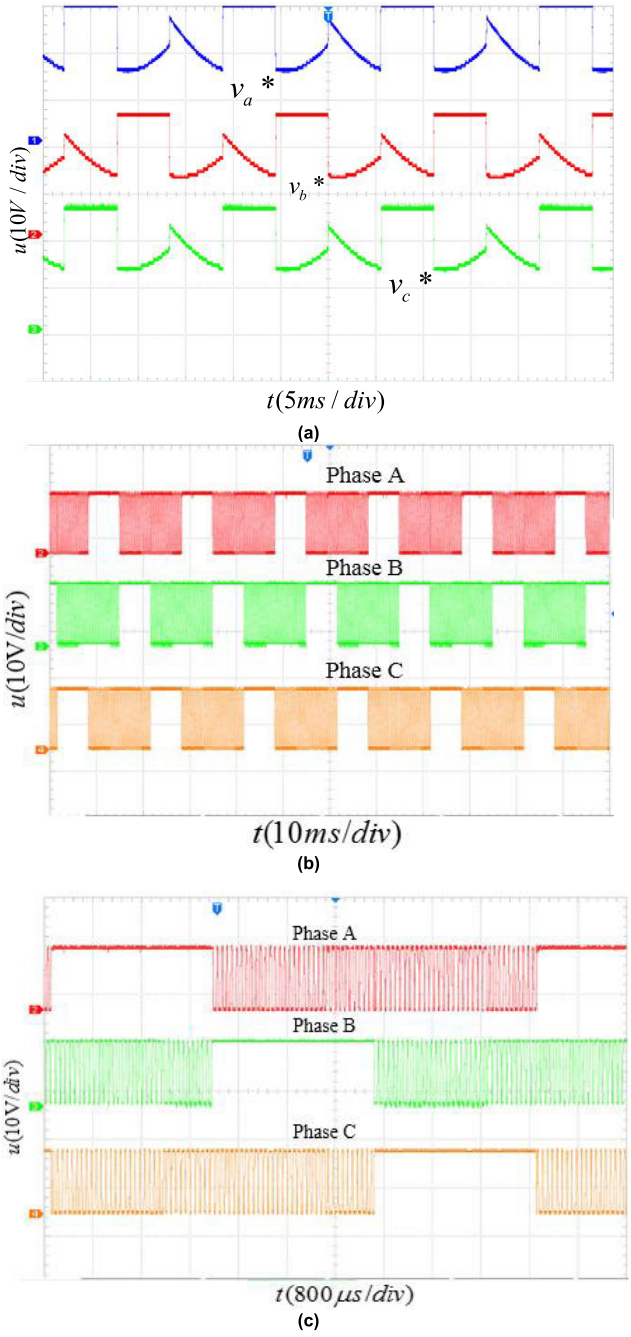

FIGURE 18. Experimental waveforms of the equivalent SVPWM (a) the new three-phase modulation signals (b) the three switching pulses (c) the enlarged view of switching pulses.

By analyzing the experimental waveform of three-phase novel modulation wave shown in Fig. 18(a), based on the expression in Table 4 and simulation waveform in Fig. 14, it can be found that the feasibility of proposed equivalent 12-sector modulation is verified by the experimental waveforms, and the experimental results are consistent with the theoretical derivation and simulation waveforms. The three output switching pulses are shown in Fig. 18(b), and Fig. 18(c) is

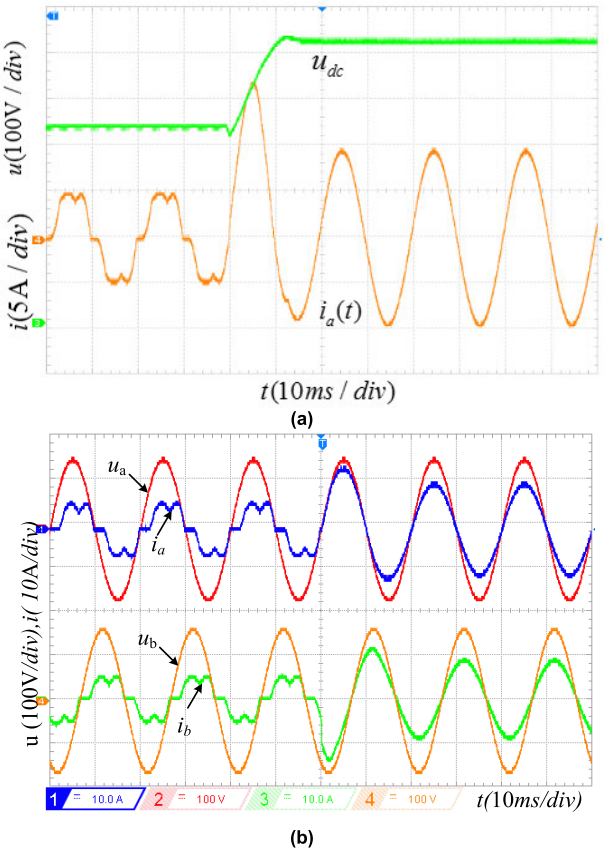

FIGURE 19. Three-phase PFC dynamic voltage and current related waveform (a) Phase A dynamic current waveform and DC side voltage waveform (b) Phase A and Phase B dynamic voltage and current waveform.

the partial amplification, It can be seen that the three-phase switch pulse distribution is consistent with the theoretical analysis in Fig. 15.

From top to bottom of the Fig. 19, which are the waveform of DC side voltage and phase-A current when three-phase PFC is started, and the waveform of dynamic voltage and current are shown from uncontrolled state to controlled state. In Fig. 19(a), the DC side voltage can reach a stable value of 650V in about a source cycle, it has small overshoot and good dynamic response. In Fig. 19(b), the steady-state operation can be quickly realized when the three-phase PFC is started, and the voltage and current are in the same phase.

The voltage and current waveforms of the Y-type two-level PFC in steady state are shown in Fig. 20, which verify the working characteristics of the studied PFC. It can be seen from Fig. 20(a) that the voltage waveforms of phase voltage and line voltage conform to the characteristics of Y-type two-level PFC, and in stable state, the three-phase input current can be highly sinusoidal, with low harmonic content and only a small amount of lower harmonic, and the input line voltage is three-level, which is consistent with the above-mentioned analysis.

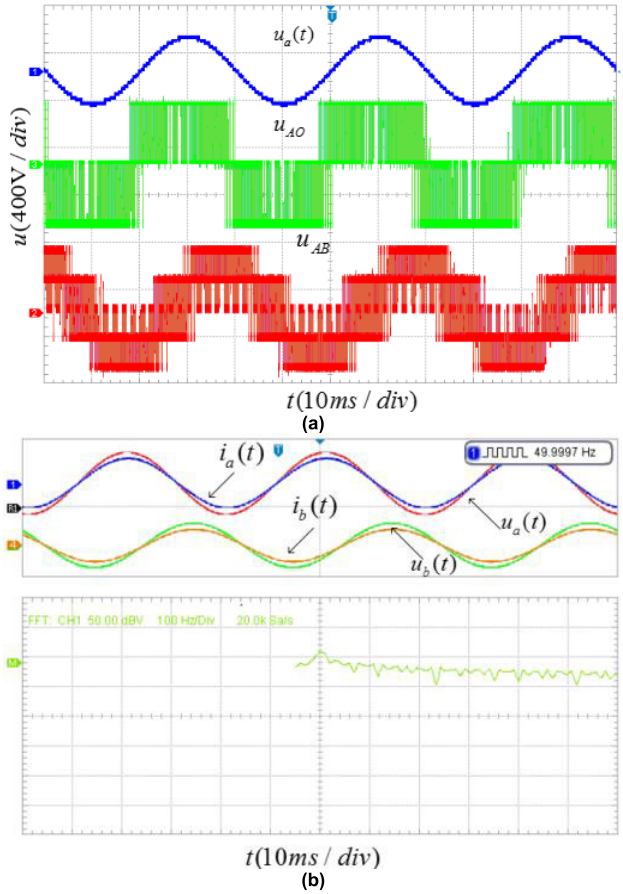

FIGURE 20. Three-phase PFC steady-state voltage and current related waveform (a) three Phase PFC phase voltage and line voltage input waveform, (b) harmonic analysis of A-phase current in steady state.

VI. CONCLUSION

In this paper, the three-phase/switch Y-type two-level rectifier was studied in detail. Compared with three-phase PWM rectifier, the three-phase/tube two-level Y-type PFC can effectively reduce the number of switching devices and the switching loss, and this PFC circuit has high engineering value in unidirectional power applications. Furthermore, based on the virtual vectors and the operation principle of three-phase/switch two-level PFC, this paper proposed 12-sector SVPWM and equivalent 12-sector SVPWM for this circuit. Since the virtual vectors can reduce the error between the reference voltage vector and the synthetic target vector, which does not need sector judgment and vector action time solution. The equivalent 12-sector SVPWM can reduce computational processing time which is its simplicity for digital implementation, and this virtual 12-sector equivalent SVPWM technique can be applied in traditional three-phase three-level rectifiers. Finally, the simulation and a 5kW experimental topology are designed to verify the capability of the proposed two 12-sector SVPWM strategies.

REFERENCES

[1] F. Yu, X. Liu, X. Zhang, and Z. Zhu, "Model predictive virtual-flux control of three-phase vienna rectifier without voltage sensors," *IEEE Access*, vol. 7, pp. 169338–169349, 2019.
[2] O.-A. Tubburee and Y. Kumsuwan, "Discontinuous gate-drive signals for a three-phase three-switch unidirectional delta-type rectifier based on 2L-SVM analysis of a vienna rectifier," in *Proc. Int. Electr. Eng. Congr. (iEECON)*, Pattaya, Thailand, Mar. 2017, pp. 1–4.
[3] B. Tan, Z. Gu, K. Shen, and X. Ding, "Third harmonic injection SPWM method based on alternating carrier polarity to suppress the common mode voltage," *IEEE Access*, vol. 7, pp. 9805–9816, 2019.
[4] Y. He, Y. Liu, C. Lei, and J. Liu, "Equivalent space vector output of diode clamped multilevel inverters through modulation wave decomposition under carrier-based PWM strategy," *IEEE Access*, vol. 8, pp. 104918–104932, 2020.
[5] J. Chen, Y. He, S. U. Hasan, and J. Liu, "A comprehensive study on equivalent modulation waveforms of the SVM sequence for three-level inverters," *IEEE Trans. Power Electron.*, vol. 30, no. 12, pp. 7149–7158, Dec. 2015.
[6] J. Liang, H. Wang, and Z. Yan, "Grid voltage sensorless model-based predictive power control of PWM rectifiers based on sliding mode virtual flux observer," *IEEE Access*, vol. 7, pp. 24007–24016, 2019.
[7] Y. Li and H. Zhao, "A space vector switching pattern hysteresis control strategy in VIENNA rectifier," *IEEE Access*, vol. 8, pp. 60142–60151, 2020.
[8] W. Chen, H. Sun, X. Gu, and C. Xia, "Synchronized space-vector PWM for three-level VSI with lower harmonic distortion and switching frequency," *IEEE Trans. Power Electron.*, vol. 31, no. 9, pp. 6428–6441, Sep. 2016.
[9] H. Ma, Y. Xie, and Z. Shi, "Improved direct power control for vienna-type rectifiers based on sliding mode control," *IET Power Electron.*, vol. 9, no. 3, pp. 427–434, Mar. 2016.
[10] S.-W. An, S.-M. Kim, and K.-B. Lee, "Optimized space-vector modulation to reduce neutral point current for extending capacitor lifetime in three-level inverters," *IEEE Access*, vol. 8, pp. 97689–97697, 2020.
[11] B. Zhu, F. Ding, and D. M. Vilathgamuwa, "Coat circuits for DC–DC converters to improve voltage conversion ratio," *IEEE Trans. Power Electron.*, vol. 35, no. 4, pp. 3679–3687, Apr. 2020.
[12] H. Fang, X. Ge, W. Song, R. Ding, and X. Feng, "Relationship between two-level space-vector pulse-width modulation and carrier-based pulse-width modulation in the over-modulation region," *IET Power Electron.*, vol. 7, no. 1, pp. 189–199, Jan. 2014.
[13] J. Wang, Z. Gui, P. Wang, J. Wang, and W. Jiang, "A carrier-based modulation with planned zero sequence voltage injection to control neutral point voltage for three-level inverter," *IEEE Access*, vol. 8, pp. 64799–64809, 2020.
[14] C. Wang, T. Tian, Z. Xu, S. Cheng, S. Liu, and R. Chen, "Optimal management for grid-connected three/single-phase hybrid multimicrogrids," *IEEE Trans. Sustain. Energy*, vol. 11, no. 3, pp. 1870–1882, Jul. 2020, doi: 10.1109/TSTE.2019.2945924.
[15] J.-S. Lee and K.-B. Lee, "Carrier-based discontinuous PWM method for vienna rectifiers," *IEEE Trans. Power Electron.*, vol. 30, no. 6, pp. 2896–2900, Jun. 2015.
[16] B. Zhu, Q. Zeng, Y. Chen, Y. Zhao, and S. Liu, "A dual-input high step-up DC/DC converter with ZVT auxiliary circuit," *IEEE Trans. Energy Convers.*, vol. 34, no. 1, pp. 161–169, Mar. 2019.
[17] C. Wang, H. Hu, H. Cheng, Z. Zhao, and J. Liu, "Voltage balancing control of cascaded single-phase VIENNA converter based on one cycle control with unbalanced loads," *IEEE Access*, vol. 8, pp. 95126–95136, 2020.
[18] W. Zhu, C. Chen, and S. Duan, "Model predictive control with improved discrete space vector modulation for three-level vienna rectifier," *IET Power Electron.*, vol. 12, no. 8, pp. 1998–2004, Jul. 2019.
[19] C. Wang, X. Li, T. Tian, Z. Xu, and R. Chen, "Coordinated control of passive transition from grid-connected to islanded operation for three/single-phase hybrid multimicrogrids considering speed and smoothness," *IEEE Trans. Ind. Electron.*, vol. 67, no. 3, pp. 1921–1931, Mar. 2020.
[20] H. Ma, M. Feng, Y. Tian, and X. Chen, "Research on carried-based PWM with zero-sequence component injection for vienna type rectifiers," *J. Power Electron.*, vol. 19, no. 2, pp. 560–568, 2019.

HUI MA (Member, IEEE) was born in Kaifeng, Henan, China, in 1985. He received the M.S. degree in electrical engineering and automation from the Changchun University of Technology, Jilin, China, in 2013, and the Ph.D. degree in power electronics from the School of Electric Power, South China University of Technology, Guangzhou, China, in 2016. Since 2016, he has been an Assistant Professor with the College of Electrical Engineering and New Energy, China Three Gorges University, Yichang. His current research interests include high-power density rectifiers, multilevel converters, and electric energy conversion control strategies in various industrial fields. He used to serve as a Reviewer for journals, such as *IET Power Electronics* and the *Journal of Power Electronics*.

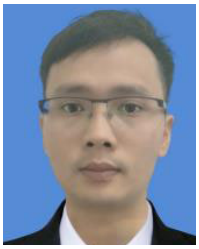

YUN LU was born in Huanggang, Hubei, China, in 1988. He received the B.S. degree in automation and the M.S. degree in electrical engineering and automation from China Three Gorges University, Yichang, China, in 2012 and 2015, respectively. His current research interests include high-power density rectifiers, multilevel converters, and electric energy conversion control strategies in various industrial fields.

KAITONG ZHENG was born in Henan, China, in 1994. He received the B.S. degree in electrical engineering from the Henan University of Urban Construction, Pingdingshan, China, in 2019. He is currently pursuing the M.D. degree in power electronics with the College of Electrical Engineering and New Energy, China Three Gorges University, Yichang, China. His current research interests include multilevel converters and control algorithms.

TIANCHUAN XU was born in Xianning, Hubei, China, in 1998. She received the B.E. degree in smart grid information engineering from the Qingdao University of Science and Technology, in 2020. She is currently pursuing the M.D. degree with the Department of Electricity and New Energy, China Three Gorges University. Her current research interests include multilevel rectifier and power factor correction rectifier.